Received: 12 March 2025 | Revised: 19 May 2025 | Accepted: 9 June 2025

DOI: 10.1002/pro.70206

RESEARCH ARTICLE

THE PROTEIN SOCIETY WILEY

Allosteric regulation of L-lactate dehydrogenase: Beyond effector-mediated tetramerization

Hanfeng Cai[1] | **Smadar Shulami**[1] | **Zoran Štefanić**[2] | **Tomica Hrenar**[3] | **Aleksandra Maršavelski**[3] | **Ayelet Fishman**[1]

[1]Department of Biotechnology and Food Engineering, Technion-Israel Institute of Technology, Haifa, Israel

[2]Division of Physical Chemistry, Ruđer Bošković Institute, Zagreb, Croatia

[3]Department of Chemistry, Faculty of Science, University of Zagreb, Zagreb, Croatia

Correspondence
Aleksandra Maršavelski, Department of Chemistry, Faculty of Science, University of Zagreb, Horvatovac 102a, 10000 Zagreb, Croatia.
Email: amarsavelski.chem@pmf.hr

Ayelet Fishman, Department of Biotechnology and Food Engineering, Technion-Israel Institute of Technology, Haifa 3200003, Israel.
Email: afishman@technion.ac.il

Funding information
Croatian Science Foundation, Grant/Award Number: IP-2019-04-6764; Israel Science Foundation, Grant/Award Number: 1372/24; European Cooperation in Science and Technology, Grant/Award Number: CA21162; Development Research Support (NextGenerationEU), Grant/Award Number: NPOO.C3.2.R2-I1.06.0041; European Regional Development Fund-Competitiveness and Cohesion Operational Programme, Grant/Award Number: KK.01.1.1.02.0016

Review Editor: Nir Ben-Tal

Abstract

The activity of allosterically regulated enzyme is modulated through structural changes induced by effectors. L-lactate dehydrogenase from *Geobacillus stearothermophilus* (GsLDH) catalyzes the reversible conversion between pyruvate and lactate using NAD(H), and its activity is known to be activated by fructose 1,6-bisphosphate (FBP). However, the molecular basis of this regulation has not been explored using molecular dynamics (MD) simulations. In this study, we integrated MD simulations with biochemical assays to investigate the impact of FBP on GsLDH structure and function. MD revealed that FBP stabilizes the tetrameric form, reduces residue flexibility, and enhances pyruvate interactions with active site residues, despite a 23 Å distance between binding sites. Using MDavocado, we identified three *P*-axis-related dimer interface regions critical for stability and structural integrity. Microcalorimetry titration revealed that NADH binding ($K_d = 1.2 \pm 0.3$ μM) occurs only in the presence of FBP, indicating an enthalpy-driven interaction involving a hydrogen-bond network. Single amino acid replacement, Gln189Leu, maintains tetrameric structure without FBP and enhances the substrate inhibition effect. However, this mutant fails to trigger the allosteric transition toward a conformation with higher affinity for the substrate, resulting in a high $K_{0.5}$ value (2.3 ± 0.2 mM) and a low $k_{cat}/K_{0.5}$ (32 ± 4 s^{-1} mM^{-1}), comparable to that of the WT without FBP. These findings suggest that oligomerization alone does not confer allosteric responsiveness, emphasizing the essential role of specific interactions in allosteric regulation. Collectively, our results advance the molecular understanding of FBP as a key allosteric effector to stabilize quaternary structure and improve enzyme activity.

KEYWORDS
allosteric regulation, fructose 1,6-bisphosphate, *Geobacillus stearothermophilus*, lactate dehydrogenase, microcalorimetric titration, molecular dynamics

1 | INTRODUCTION

Allosteric regulation of enzymes refers to a process in which enzyme activity or structural features are modulated in response to the binding of an effector molecule (Astore et al., 2024; McCullagh et al., 2024). Two primary models have been proposed to describe the allosteric mechanism: the Koshland–Némethy–Filmer (KNF) model and the Monod–Wyman–Changeux (MWC) model (Monod et al., 1965). The MWC model, also known as the concerted model, posits that a protein is in a pre-existing equilibrium between two

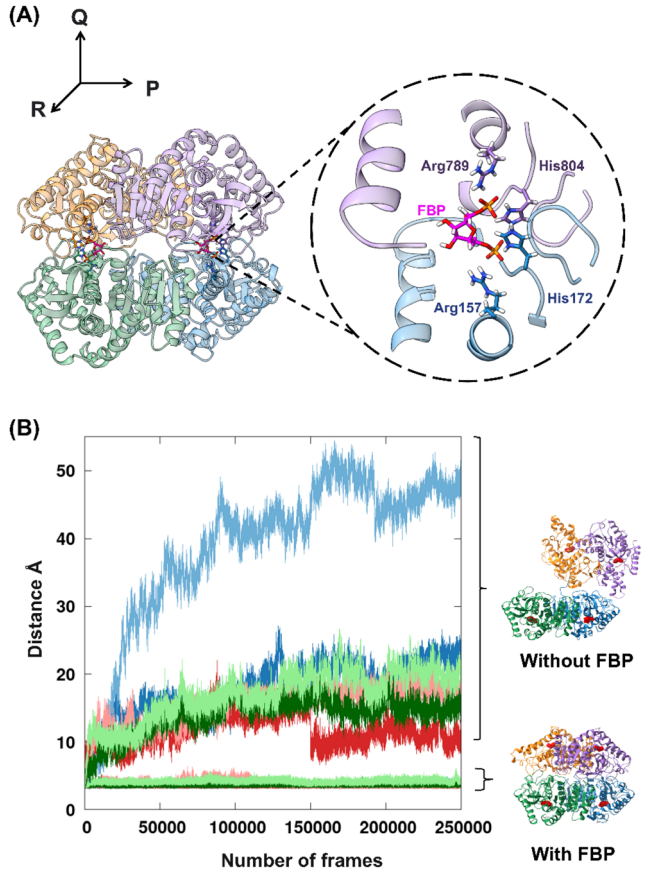

FIGURE 1 Changes in oligomeric states captured by MD simulations. (a) Tetrameric structure of GsLDH is represented by a ribbon diagram, with four identical subunits colored blue, purple, yellow, and green. One of the FBP-binding sites of GsLDH, which consists of four positively charged residues, His172 and Arg157 from SUB1 (blue) and His804, Arg789 from SUB3 (purple). The second FBP-binding site is located between SUB2 (orange) and SUB4 (green). (b) The distance between center of mass of histidine side chains from the two *P*-axis-related dimers with and without FBP. Three replicates are colored in blue, red and green. The distances between SUB1 and SUB3 are marked in dark colors and SUB2 and SUB4 are marked in light colors.

conformational states: T (tensed, inactive) and R (relaxed, active). Even in the absence of an allosteric modulator, these states coexist, and the binding of an allosteric modulator shifts the equilibrium in a concerted manner, promoting the active state (Brunori & Miele, 2023; Wu et al., 2024). In contrast, the KNF model, or sequential model, proposes that the binding of an allosteric modulator induces conformational changes in the protein that sequentially alter its affinity for ligand. This results in incremental changes in activity as each subunit's conformation is modified individually.

To study the allosteric response, we chose L-lactate dehydrogenase (LDH, EC 1.1.1.27), a pivotal enzyme involved in anaerobic metabolism, catalyzing the conversion of pyruvate to lactic acid, using NAD(H) as a cofactor (Robin et al., 2023). Bacterial LDHs are typically homotetrameric and are often subjected to allosteric regulation by fructose 1,6-bisphosphate (FBP). The tetrameric structure is organized along three axes P, Q, and R, with two FBP molecules bound at the interface between two *P*-axis dimer units (Figure 1a). Each of the two FBP molecules neutralizes the local net positive charge of histidine and arginine from two adjacent subunits, by forming salt bridges with the phosphate groups of FBP (Figure 1a). The binding of FBP facilitates the transition from the T to the R state, as proposed in the MWC model (Thirumalai et al., 2019). Structural comparison among LDHs revealed distinct differences in their 3D structures and ligand-binding sites, highlighting significant diversity in the allosteric mechanisms of bacterial LDHs (Bertrand et al., 2023; Coquille et al., 2025; Taguchi, 2017). However, these comparative studies often overlook crucial aspects of the protein's flexibility, conformational changes, and dynamic behaviors that underlie allosteric phenomena. For example, while the MWC model is widely accepted, it does not fully explain ligand-induced allostery based solely on experimental or structural data. Recent in silico simulations have provided valuable insights into the interface residues that drive allosteric transitions and regulate LDH assembly (Chen & Thirumalai, 2018). Structural perturbation analysis has shown that the transition from the T to R state is mediated by a network of key residues, known as the allosteric wiring diagram, located at the subunit interfaces (Chen & Thirumalai, 2018). These residues play a crucial role in allosteric regulation and contribute to the assembly of LDH monomers. Additionally, quantitative measurements revealed that the allosteric transition is accompanied by a rotation of the subunits (Chen & Thirumalai, 2018).

The lactate dehydrogenase from *Geobacillus stearothermophilus* (GsLDH, formerly known as bsLDH) is an allosterically regulated enzyme whose kinetic properties, substrate affinity, catalytic efficiency, and structure-based studies have been comprehensively characterized (Aslan et al., 2016; Binay et al., 2009; Binay et al., 2013; Nie et al., 2016). Structural studies have shown that proper orientation of catalytic residues such as Arg92, Arg155, and His179 is essential for substrate positioning and redox catalysis in GsLDH (Aslan et al., 2016). These interactions are preserved in engineered variants and modulated by flexible loop dynamics. Additionally, Arg155 is repositioned by allosteric binding of FBP, enhancing its interaction with the substrate and highlighting the role of conformational control in catalysis (Binay et al., 2009).

However, these studies lack molecular dynamic (MD)-based analyses, demonstrating oligomeric state transitions, conformational changes, residues flexibilities, and revealing specific network interactions governing allosteric regulation. In this study, we combined MD simulations with biochemical analyses, providing

novel and uncharacterized insights into the impact of FBP on the oligomeric state of GsLDH, as well as its substrate and cofactor affinity. Using the innovative MDavocado tool, we identified three key regions that undergo significant conformational shifts between the T state (without FBP) and the R state (with FBP), highlighting critical structural transitions. We show that a single replacement in the interface stabilizes FBP-independent tetramerization and increases substrate inhibition through a yet uncharacterized mechanism. Furthermore, isothermal titration calorimetry (ITC) measurements support the role of FBP in promoting hydrogen-bond formation and stabilizing enzyme-cofactor interactions. These findings provide new mechanistic insights into allosteric regulation and demonstrate that oligomerization alone is insufficient to drive allosteric responsiveness.

2 | RESULTS

2.1 | MD simulations capture oligomeric state change influenced by FBP

The FBP-binding site of GsLDH consists of four positively charged residues, His172, Arg157, and His804, Arg789 from *P*-axis-related subunits (Figure 1a). The binding of FBP significantly influences the conformational state of GsLDH by modulating electrostatic interactions between positively charged residues at the FBP-binding site. Specifically, in the absence of FBP, the repulsive interactions between the positively charged residues His172, Arg157 and His804, Arg789 from the *P*-axis-related subunits lead to the dissociation of the tetrameric enzyme into two dimers, driven by charge repulsion (Supplementary video S2). However, upon FBP binding, these repulsive forces are eliminated, facilitating the transition from the open T state to the closed R state (Clarke, Waldman, et al., 1985) and the maintenance of a tetrameric state (Supplementary video V2). To track the oligomerization process, we measured the distance of His172 between two *P*-axis-related dimers during the MD simulation. In the presence of FBP, the distances between SUB1/SUB3 and SUB2/SUB4 stabilized at an average of 3.5 and 3.8 Å, respectively, indicating the maintenance of the tetrameric structure (Figure 1b). However, when the simulation was run without FBP, there was a gradual increase in the distance between the subunits, exceeding 20 Å, suggesting the disruption of the tetrameric assembly (Figure 1b).

2.2 | Residue flexibility is reduced in the presence of FBP

To quantify the flexibility of residues during the oligomerization process, along trajectories, we calculated

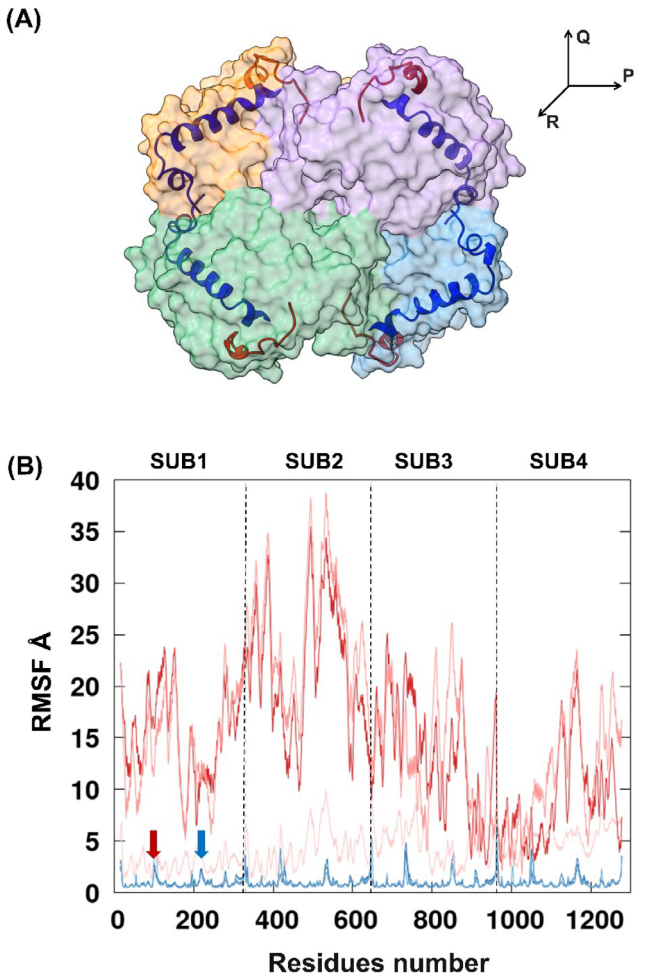

FIGURE 2 Residues flexibility upon FBP binding. (a) Active loops (shown in red) located in the pyruvate-binding sites are flexible regions that switch between an open and closed form to accommodate the substrate. Mobile *α*-helices (in blue) are located at the *P*-axis inter-subunit contact regions. (b) RMSF values of C*α*, N, C, O backbone atoms across all residues in WT GsLDH are presented. MD simulation with FBP is shown in blue and without FBP is presented in red. The triplicates are shown in different red and blue intensities. Two fluctuation regions, corresponding to the active site loop (residues 81–96) and the mobile *α*-helix (residues 195–226) are shown in red and blue arrows, respectively.

the root mean square fluctuation (RMSF). The crystal structure of GsLDH reveals an active site loop (residues 81–96) located at the pyruvate-binding site, which serves as a flexible region that transitions between open and closed conformations to accommodate the substrate (Figure 2a). Additionally, a mobile *α*-helix (residues 195–226) situated at the *P*-axis inter-subunit contact region is exposed to the solvent, allowing it to remain dynamic during allosteric regulation (Figure 2a). We hypothesized that, in the presence of FBP, the overall flexibility of the protein's residues would remain stable (low RMSF values), except at these identified flexible regions. As demonstrated in Figure 2b, the MD simulation in the presence of FBP resulted in low

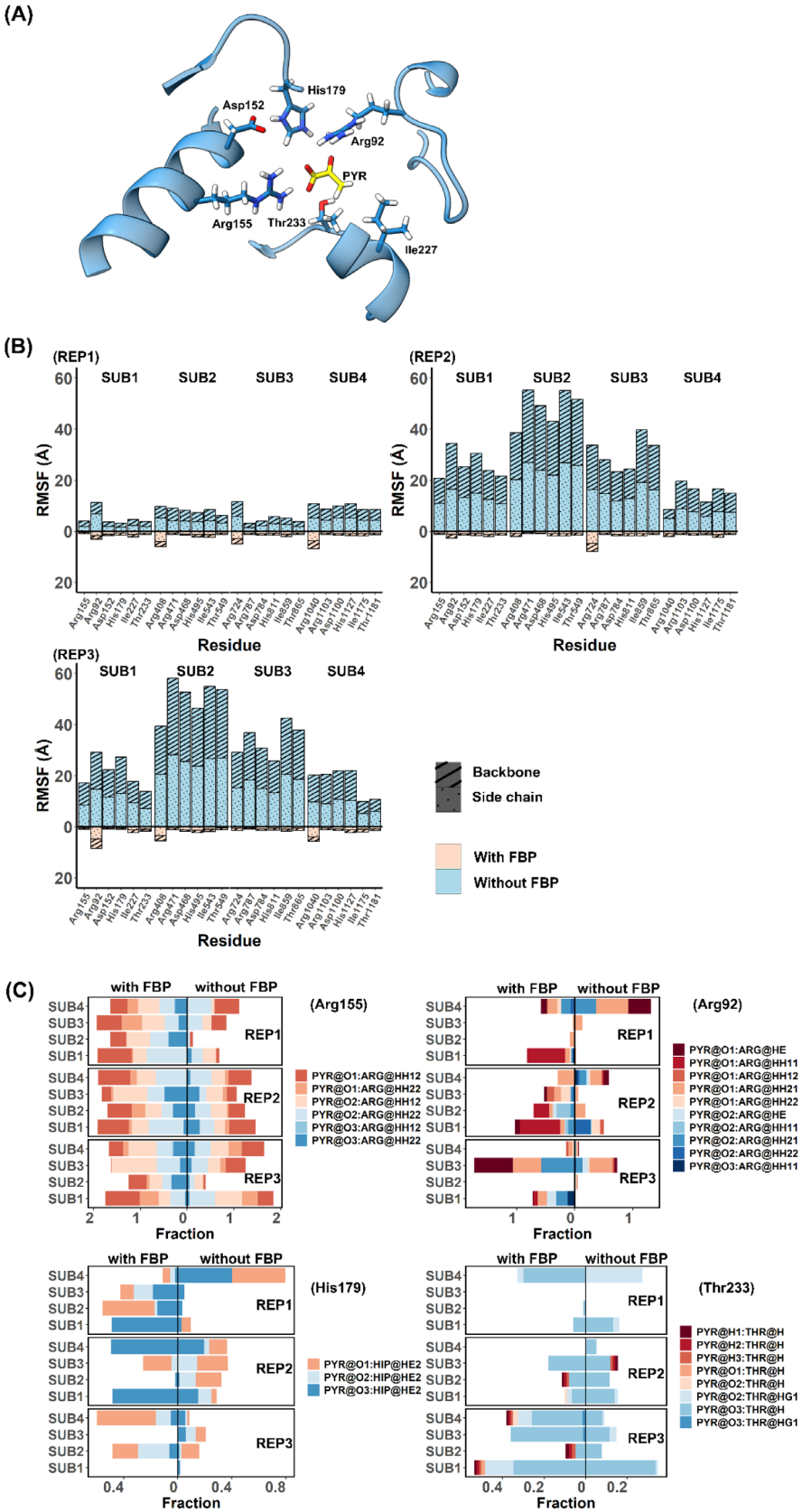

FIGURE 3 FBP stabilizes the binding of pyruvate by reducing residue fluctuation and enhancing hydrogen bond formation. (a) Pyruvate binding pocket in GsLDH; (b) RMSF value of six residues in the pocket for three replicas; (c) Occupancy of hydrogen bond interactions between pyruvate and residues Arg155, Arg92, His179, Thr233 in GsLDH across simulation frames.

RMSF values (<5 Å), with consistent and repeatable dynamic patterns across all four subunits. Notably, the two regions exhibited increased fluctuations, corresponding to the active site loop and the mobile α-helix, reflecting their crucial roles in the enzyme's functionality. In the absence of FBP, dissociated subunits

exhibited a non-crystallographic pattern of fluctuations, resulting in residues with higher RMSF values, which indicate greater flexibility and conformational variability (Figure 2b).

2.3 | Quantification of residue flexibility and hydrogen bonds involved in pyruvate stabilization upon FBP binding

We further focused on the analysis of the pyruvate-binding site with particular emphasis on six specific residues involved in pyruvate binding. Arg155 and Thr233 form hydrogen bonds with the carboxyl group of pyruvate, facilitating substrate binding and orientation. Additionally, Arg92, located on the active site loop, polarizes the carbonyl group of pyruvate, facilitating the proton transfer from His179. Finally, Asp152 and Ile227 contribute to maintaining the stability of the binding pocket (Figure 3a).

To analyze the impact of FBP binding on the pyruvate binding site, we conducted a detailed analysis of the RMSF values for the six specific residues that are critical for pyruvate binding. These RMSF values provide insight into the flexibility and conformational variability of the residues throughout the course of the MD simulations.

We compared the RMSF values obtained from simulations carried out with FBP present to those from simulations without FBP. This comparative approach allowed us to identify any changes in the dynamics of the residues in response to FBP binding, which may influence the overall flexibility and conformation of the pyruvate binding site.

Notably, the FBP binding site is located 23 Å away from the pyruvate binding site (Figure S1), suggesting that any conformational changes induced by FBP binding could potentially propagate through the protein structure, affecting the pyruvate binding site even at that distance. In general, five residues exhibited minimal fluctuations in the presence of FBP. As expected, Arg92 showed high fluctuations due to its position on the active loop. In the absence of FBP, all analyzed residues in the pyruvate binding site displayed significantly high fluctuations, indicating that the pyruvate active site features enhanced conformational freedom (Figure 3b). This implies that binding of FBP ensures appropriate stability of the pyruvate binding site. Furthermore, we quantified the occupancy of hydrogen bond formation between pyruvate and four residues (Arg155, Arg92, His179, and Thr233) along the simulation trajectories. For each residue, the fractions of hydrogen bonds formed with pyruvate were accumulated to represent the overall interaction (Figure 3c). In the absence of FBP, the enzyme lost most hydrogen bond interactions between Arg155 and pyruvate. Similar decreases in hydrogen bonding were observed for Arg92, His179, and Thr233.

2.4 | Analysis of conformational changes modulated by FBP

To identify key residues exhibiting distinct dynamics in MD simulations conducted both in the presence and absence of FBP, we utilized the MDavocado tool (Gomaz et al., 2024) for a comprehensive analysis. This assessment focused on examining the overall distribution of main-chain and side-chain conformations, visualized through Ramachandran plots (φ–ψ diagrams) and Janin plots ($\chi1$–$\chi2$ diagrams). Our analysis revealed a high degree of similarity among the four subunits of GsLDH. In particular, we observed that most protein regions maintained consistent conformations when FBP was present, suggesting that FBP plays a vital role in stabilizing the enzyme's structure. The Ramachandran plots demonstrated that the backbone torsion angles (φ and ψ) for most residues were clustered within favored regions, indicating a stable and optimally folded conformation in the presence of FBP. Furthermore, the Janin plots provided deeper insights into the distribution of side-chain conformations ($\chi1$ and $\chi2$), reinforcing our observation of uniformity across the subunits. The binding of FBP appears to enhance the structural integrity of critical residues, likely contributing to improved interactions and reduced mobility of the enzyme. In contrast, in the absence of FBP, we noted significant conformational changes in three key regions at the *P*-axis dimer interface. These alterations were characterized by quantifying the dihedral angles (φ, ψ, $\chi1$, $\chi2$) of the affected residues, which are summarized in Table 1. The alterations observed in these regions suggest that the loss of FBP binding leads to increased flexibility and variability, potentially compromising the enzyme's functionality and structural cohesion. The first region of interest involves Asn170, which is located within the FBP-binding site and is oriented toward Ile255 of the *P*-axis-related subunit. In the presence of FBP, both residues adopt distinct and stable conformations, as illustrated in Figure 4. However, when FBP is absent, Asn170 exhibits multiple side-chain conformations, characterized by variations in its $\chi1$ and $\chi2$ angles. This increased variability suggests that the absence of FBP leads to a loss of stabilizing interactions, resulting in a less defined orientation for Asn170. In contrast, Ile255 exhibits only a slight shift in its φ angle, moving from $-90°$ to $-83°$, indicating that while it remains relatively stable, there is still some conformational flexibility in the absence of its allosteric modulator.

The second region encompasses Lys60, which is situated at the junction between helix αC and strand βC, as well as His250 located on the α3G helix of the diagonal subunit (Figure 4b). In the absence of FBP, the Janin plots for these residues show dispersed clusters, indicating a lack of structural coherence. This stands in stark contrast to the tight and focused

TABLE 1 Dihedral angles ($\varphi, \psi, \chi1, \chi2$) of the identified residues determined with MDavocado.

		Asn170	Ile255	Lys60	His250	Ala190	Tyr191	Ile193	Val194
With FBP	φ	−81	−90	−139	−90	−142	−144	−111	−124
	ψ	−12	125	146	2	135	151	106	−16
	$\chi1$	−64	−62	−174	−62	-	−44	−62	−62
		-	-	63	-	-	-	-	68
	$\chi2$	107	152	178	−89	-	−85	173	-
		−74	-	−69	−84	-	93	−60	-
Without FBP	φ	−80	−83	−136	−92	−105	−143	−121	−107
	ψ	−22	121	144	4	126	156	117	−14
	$\chi1$	−62	−63	−175	−63	-	−50	−61	−61
		−168	-	65	−160	-	64	177	72
		-	-	−68	-	-	-	-	−175
	$\chi2$	101	164	148	−173	-	−91	172	-
		−101	74	79	−95	-	92	−61	-
		25	-	−71	72	-	-	-	-

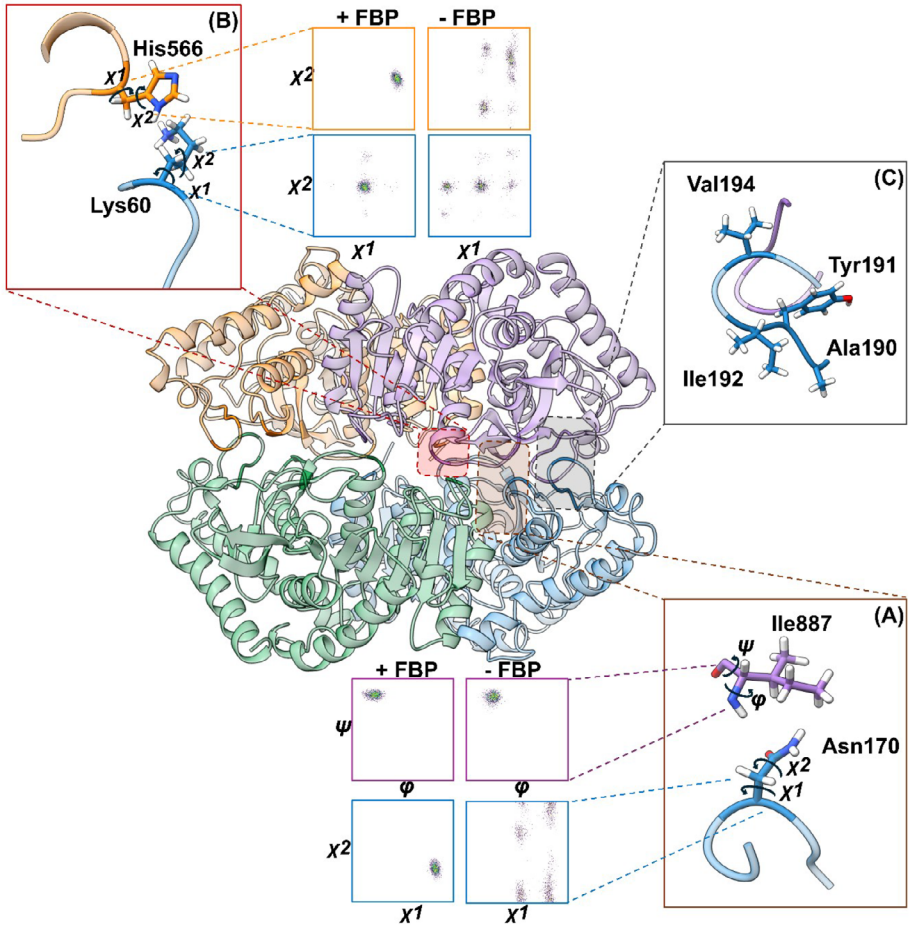

FIGURE 4 Analyzing conformational changes modulated by FBP. Three highlighted regions that exhibit distinct dynamics in MD simulations were identified by MDavocado analysis. (a) The region involves Asn170, located within the FBP-binding site and oriented toward Ile255 of the *P*-axis-related subunit. (b) The region includes Lys60, situated at the junction between helix αC and strand βC, as well as His250 on the α3G helix of the diagonal subunit. (c) The region consists of a predominantly hydrophobic loop formed by Ala190, Tyr191, Ile192, and Val194, which connects βC and αT at the *P*-axis dimer interface. The inner panels are Ramachandran plots (φ–ψ diagrams) and Janin plots ($\chi1$–$\chi2$ diagrams) for identified residues with their corresponding dihedral angles marked.

TABLE 2 Kinetic constants and oligomeric state determination for WT GsLDH and its variants, with and without bound FBP.

GsLDH variants	K_m or $K_{0.5}$ (mM)		k_{cat} (s^{-1})		k_{cat}/K_m or $k_{cat}/K_{0.5}$ (s^{-1} mM^{-1})		K_i (mM)		n (Hill coefficient)		Oligomeric state[a]	Size (kDa)
	-	FBP	-	FBP	-	FBP	-	FBP	-	FBP		
WT	2.8 ± 0.4	0.5 ± 0.1	118 ± 34	64	43 ± 13	144 ± 67	ND	6 ± 1	1.5 ± 0.1	ND	Dimer	80
Triple mutant[b]	0.41 ± 0.09	0.6 ± 0.1	57 ± 8	94	141 ± 18	156 ± 59	ND	1.4 ± 0.4	ND	ND	Tetramer	120
Gln189Leu	2.3 ± 0.2	0.8 ± 0.1	73 ± 12	83	32 ± 4	106 ± 19	ND	0.3 ± 0.1	1.4 ± 0.1	ND	Tetramer	106

Note: In the presence of FBP, all the kinetic observations (WT, Gln189Leu, and Arg104Cys/Gln189Leu/Asn293Ser) were fitted by the Michaelis–Menten equation with substrate inhibition. In the absence of FBP, the Hill equation was used for both WT and Gln189Leu since they exhibited a sigmoidal curve (Supporting Figure S2). For the triple mutant Arg104Cys/Gln189Leu/Asn293Ser, a standard Michaelis–Menten equation was applied.
Abbreviation: ND, not detected.
[a]Oligomeric state was determined in the absence of FBP, using size exclusion chromatography.
[b]Triple mutant: Arg104Cys/Gln189Leu/Asn293Ser.

distributions observed in the presence of FBP, which implies a more rigid and defined environment for these residues when the modulator is bound. The increased dispersion of their conformations reflects a heightened degree of conformational flexibility, with both Lys60 and His250 displaying multiple dihedral angles for $\chi 1$ and $\chi 2$ when FBP is absent. The third region highlights a predominantly hydrophobic loop formed by Ala190, Tyr191, Ile192, and Val194, which connects βC and αT at the *P*-axis dimer interface (Figure 4c). In the absence of FBP, Ala190 undergoes a significant backbone conformational change, evident from its φ angle shifting from -142° to -105° and its ψ angle changing from 135° to 126° (Table 1). This indicates that Ala190 becomes more flexible in the absence of FBP, potentially destabilizing the hydrophobic interactions that are crucial for maintaining the integrity of the dimer interface. While the main-chain dihedral angles of Tyr191, Ile192, and Val194 remain relatively unchanged, their side-chain conformations exhibit greater flexibility, as shown by increased variability in the $\chi 1$ and $\chi 2$ angles. This variability suggests that the overall hydrophobic character of the loop may be compromised when FBP is absent, further impacting the stability of the *P*-axis dimer interface.

2.5 | A single amino acid substitution induces FBP-independent tetramerization

We further demonstrated that in the presence of FBP, the half-substrate saturation constant (K_m) for pyruvate decreases by 5.6-fold for wild-type (WT) GsLDH, while the catalytic efficiency (k_{cat}/K_m) improves by 3.3-fold (Table 2, Figure S2). Additionally, in the absence of FBP, the enzyme adopts a dimeric oligomeric state (Supplementary video V1). These findings are consistent with previous reports on WT GsLDH, indicating that FBP induces enzyme tetramerization and enhances enzyme catalytic properties (Cameron et al., 1994; Clarke, Atkinson, et al., 1985; Clarke, Waldman, et al., 1985).

To evaluate the impact of tetramerization on catalytic efficiency, we characterized a previously reported GsLDH triple mutant that contains three specific substitutions: Arg104Cys, Gln189Leu, and Asn293Ser. This mutant retains full enzymatic activity and the same affinity toward pyruvate even in the absence of FBP (Table 2) compared to WT. However, the individual contributions of each of the mutations to the overall activity of the triple mutant have not been examined so far. Our studies demonstrate that the single Gln189Leu mutation, which is located at the dimer–dimer interface, plays a crucial role in stabilizing the tetrameric structure of the enzyme, independent of the other two mutations, Arg104Cys and Asn293Ser. Using size exclusion chromatography (Figure 5a), we demonstrated that both the Gln189Leu single mutant and the triple mutant Arg104Cys/Gln189Leu/Asn293Ser existed as tetramers in solution, even in the absence of FBP (Table 2).

Furthermore, MD simulations suggest that the Gln189Leu single mutant retains its tetrameric structure (Supplementary video V3), displaying nearly identical low RMSF values of the backbone atoms in the presence and absence of FBP (Figure 5b). These results indicate that the leucine substitution at position 189 stabilizes the tetrameric structure even when FBP is absent. However, despite maintaining its tetrameric form, the mutant shows no improvement in substrate affinity, as evidenced by a $K_{0.5}$ (half-substrate saturation constant in the Hill equation) comparable to that of the WT enzyme in the absence of FBP (Table 2, Figure S2). This finding suggests that tetramerization driven by a single substitution at position 189 is insufficient to fully restore the kinetic properties of the enzyme in the presence of the allosteric modulator FBP.

2.6 | Mutation Gln189Leu enhances substrate inhibition

The initial velocity of the reaction catalyzed by GsLDH as a function of substrate concentration exhibits typical

Michaelis–Menten behavior indicative of substrate inhibition, with kinetic constants of k_{cat}, K_m, and K_i of 64 s^{-1}, 0.5 ± 0.1 mM, and 6 ± 1 mM, respectively (Table 2, Figure S2), aligning well with previous studies (Binay & Karagüler, 2007; Hewitt et al., 1999). Notably, the substrate inhibition of the Gln189Leu mutant is 20-fold higher with a K_i value of 0.3 ± 0.1 mM compared to the WT (Table 2 and Figure 5c). Furthermore, although Gln189Leu maintains a tetrameric form without FBP, substrate inhibition occurs only in the presence of FBP, similar to the WT enzyme. These experimental findings suggest that the Gln189Leu mutation introduces significant changes in the enzyme's interaction with pyruvate. The increased substrate inhibition observed by the Gln189Leu mutant implies that certain amino acid substitutions can alter the dynamics of substrate binding and inhibition, even when those substitutions are located far from the active site. To investigate the differences in affinity for pyruvate between WT GsLDH and Gln189Leu, we calculated the enthalpy of binding for each protein variant. Additionally, we performed calculations of per-residue decomposition of the enthalpy of binding to elucidate the contributions of amino acid residues to the interactions involved in the binding process. Our calculations indicate that the Gln189Leu mutant exhibits a higher affinity for pyruvate in each subunit compared to the WT, as detailed in Supporting Tables S1a, b. This increased affinity is primarily attributed to the enhanced interactions between pyruvate and specific residues in the binding site, namely Arg92, Arg155, and His179 (Supporting Figure S3). These residues play a critical role in stabilizing the bound state of pyruvate through hydrogen bonds and ionic interactions, compared to those observed in the WT enzyme. Our analysis underscores the significance of the Gln189Leu mutation in modulating the binding characteristics of LDH toward pyruvate. Notably, even though residue Gln189 is located approximately 23 Å away from the pyruvate binding site (Supporting Figure S4), its influence on the overall binding affinity is substantial, highlighting the complex interplay of distant and local effects in enzyme-substrate interactions.

2.7 | Binding affinity of the cofactors NADH/NAD^+ in the presence of FBP

To obtain the thermodynamic parameters that are crucial for understanding the driving forces involved in cofactor binding, we applied ITC that provides a direct measure of binding enthalpy (ΔH_B), enabling the simultaneous determination of binding parameters such as the association constant (K_B), entropy (ΔS), Gibbs free energy of binding (ΔG_B), and binding stoichiometry. The ITC titration curves for the binding of NADH and NAD^+ to GsLDH in the presence of FBP are presented in Figure 6, with the thermodynamic binding parameters summarized in Table 3. All interactions were exergonic, exhibiting Gibbs free energy of binding (ΔG_B) values of approximately −8.0 kcal/mol. Titration with NAD^+, both with and without pyruvate, showed only a two-fold decrease in K_d, indicating that pyruvate does not significantly influence NAD^+ binding affinity.

The binding affinity of NADH and NAD^+ to GsLDH was confirmed to have a single binding site, as indicated by a stoichiometry value approaching $n = 1$. The dissociation constants for NADH and NAD^+ were in the micromolar range ($K_d = 1.2$ μM and 3.0 μM, respectively). Notably, titration of the enzyme with NADH or NAD^+ in the absence of FBP did not result in significant enthalpy changes. These findings highlight the necessity of FBP in facilitating the binding of GsLDH with its cofactors, emphasizing its role in stabilizing the binding site and influencing the thermodynamic properties of the enzyme-cofactor complex.

3 | DISCUSSION

Allosteric processes are driven by distinct conformational changes that effectively modulate protein activity and regulate various biological functions (Martinez-Vaz et al., 2024). Recent computational studies have demonstrated that molecular dynamics play a critical role in allostery (Astore et al., 2024). In this work, we complemented experimental kinetic studies with MD simulations to investigate the structural basis of allosteric regulation in GsLDH.

3.1 | Structural insights into the allosteric regulation of GsLDH

Oligomeric state transitions modulated by FBP. The oligomeric structure of enzymes plays a crucial role in various biological processes, including allosteric regulation, conformational stability, and thermal resistance (Lazim et al., 2021; Pasti et al., 2022; Rennie et al., 2020). Early models of allostery suggested that reversible changes in the oligomeric state of enzymes, such as shifts between dimers and tetramers, could explain cooperative regulation. Moreover, ligand binding can influence the association-dissociation equilibrium and thus enzyme activity (Frieden, 1967; Nichol et al., 1967). In the current study on GsLDH, a transition from tetramer to dimer observed via MD simulation was linked to reduced catalytic efficiency, supporting these earlier models. The enzyme's oligomeric state was also reported to depend on protein concentration, and higher pyruvate levels favored tetramer formation (Clarke, Waldman, et al., 1985; Kotik & Zuber, 1992). In the present work, kinetic data showed a sigmoidal response to pyruvate in the absence of FBP, consistent

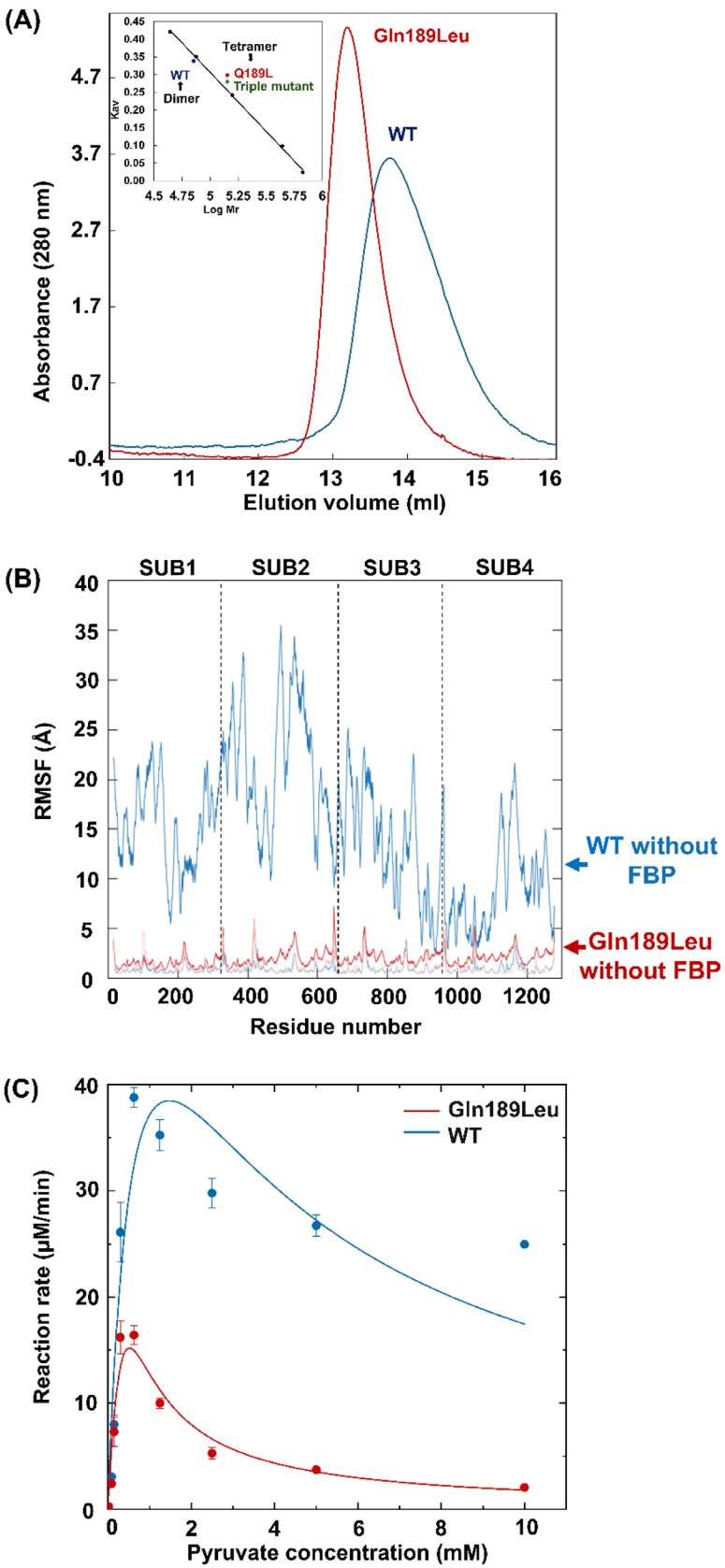

FIGURE 5 Leucine at 189 stabilizes FBP-independent tetramerization and enhances substrate inhibition. (a) Determination of the oligomeric states of GsLDHs in solution. Size exclusion chromatograms of the WT dimeric GsLDH (blue line), and the single mutant (Gln189Leu) (red line) without FBP. The inset shows the linear regression of the protein standards used for molecular weight determination (filled circles) and the position of the dimeric and tetrameric forms of GsLDH. Protein standards used were thyroglobulin (Mr, 669,000), ferritin (Mr, 440,000), aldolase (Mr, 158,000), conalbumin (Mr, 75,000) and ovalbumin (Mr, 44,000). (b) RMSF values for Cα, N, C, O backbone atoms across all residues in the Gln189Leu mutant and the WT GsLDH. RMSF values for the WT enzyme without FBP are shown in dark blue and with FBP in light blue. RMSF values for Gln189Leu mutant with and without FBP are shown in light and dark red, respectively. (c) Michaelis–Menten curves of Gln189Leu and WT GsLDH in the presence of FBP by fitting the substrate inhibition model, $V = V_{max}\, S/[K_m + S(1 + S/K_i)]$ analyzed using OriginPro 2025.

with a hysteretic system where substrate binding promotes the active tetramer (Nichol & Frieden, 1981). These results suggest that oligomerization acts as a regulatory factor, and the binding of an allosteric effector enhances substrate affinity and stabilizes the active tetrameric state.

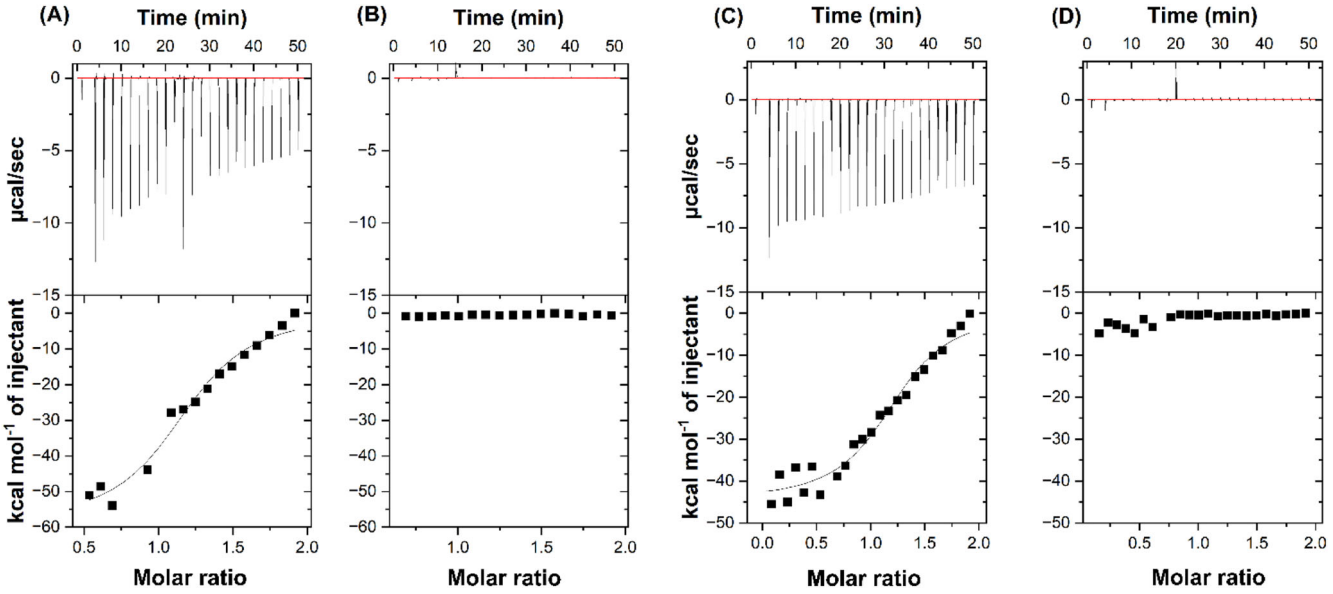

FIGURE 6 Representative isothermal calorimetric titration curves of the interactions of cofactors with GsLDH. Titration of GsLDH with NADH, in the presence of FBP (a) and without FBP (b). Titration of GsLDH with NAD^+, in the presence of FBP (c) and without FBP (d). The top panels show the calorimetric titrations of binding protein with ligand, and the bottom panels display the integrated injection heat from the top, corrected for control dilution heat. The solid lines represent the curves of best fit used to derive binding parameters. All ITC experiments were performed at 30°C.

Quantitative analysis of interactions governing allosteric regulation. Using MDavocado tool, we conducted an in-depth analysis and identified key residue interactions involved in inter-subunit communication during conformational change and oligomeric transition of GsLDH. Notably, Lys60 and His250 from the *P*-axis subunits were predominantly clustered in favorable regions, promoting electrostatic interactions and hydrogen bond formation. Additionally, stabilization of the 190–194 loop likely enhances hydrophobic interactions at the *P*-axis interface. These inter-subunit interactions are critical for maintaining structural integrity and may contribute to allosteric effects. MD simulations demonstrated that Asp152, Arg155, His179, Ile227, and Thr233 exhibit lower conformational freedom in the presence of FBP. In contrast, in the absence of FBP, Arg92 and the five mentioned residues show increased fluctuations, indicating a greater conformational variability featured by those amino acids. These six residues are highly conserved among bacterial LDHs, demonstrating their essential role in substrate stability and catalytic function (Uchikoba et al., 2002). Furthermore, our MD simulations align well with structure-based studies of LDHs, showing that Arg155 and Thr233 adopt improper conformations in the inactive T state structure (Taguchi, 2017).

Mechanistic insights into bacterial LDHs. Structural analyses revealed that non-allosteric LDHs exhibit an increased number of hydrogen bonds and salt bridges at the *Q*-axis interface, which plays a significant role in FBP-independent regulation (Arai et al., 2011; Robin et al., 2023). Moreover, non-allosteric LDHs display greater shape complementarity at subunit interfaces, with specific interactions that stabilize the R-state structure (Robin et al., 2023; Uchikoba et al., 2002). Interestingly, introducing a mutant with five amino acid substitutions to establish an inter-subunit salt bridge network enhanced FBP-independent catalysis in allosteric Lactobacillus casei LDH (Arai et al., 2011).

Bacterial LDHs exhibit two primary allosteric mechanisms. The first type, represented by BlLDH, remains tetrameric during the T-to-R transition, involving structural reorganization mediated by interfacial residues (Arai et al., 2010; Chen & Thirumalai, 2018). In contrast, the other type, such as GsLDH, shifts between a tetrameric R state and two dimers in the T state (Clarke, Waldman, et al., 1985), as confirmed here by MD simulations showing dimer dissociation in the absence of FBP. Despite these differences, both enzymes share conserved catalytic and allosteric site residues, suggesting a common mechanism involving subunit communication and structural rearrangement. The stability of the BlLDH tetramer in the T state is likely due to strong electrostatic and hydrophobic interactions at specific interfaces, which drive and stabilize its oligomeric structure.

3.2 | Leucine at position 189 stabilizes FBP-independent tetramerization

The allosteric factor FBP has a dual role. First, it promotes tetramerization by overcoming the repulsive

TABLE 3 Thermodynamic parameters of binding of cofactors to GsLDH in the presence of FBP.

Ligand	Protein sample	$K_B \times 10^5$ [M^{-1}]	K_d [μM]	ΔH_B kcal/mol	$T\Delta S_B$ kcal/mol	ΔG_B kcal/mol
NAD^+	WT with pyruvate	6 ± 2	1.6	−45 ± 2	−37.0	−8.0
	WT	3 ± 2	3.0	−142 ± 20	−134.4	−7.6
NADH	WT	8 ± 2	1.2	−59 ± 4	−50.8	−8.2

charge–charge interaction between two conserved residues, histidine, and arginine, facing each other at the subunit interface on the *P*-axis. Second, upon FBP binding, substrate affinity is significantly enhanced by an induced rearrangement of key residues in the active site. Stabilizing the FBP-independent tetrameric state without affecting catalytic properties was obtained by replacing Arg173 in the FBP binding site with glutamine (Clarke et al., 1987). This replacement stabilizes tetramerization attributed to the loss of the charge-repulsive interactions. An additional variant consisting of three mutations Arg104Cys, Gln189Leu, and Asn293Ser was shown to maintain the FBP-independent tetramerization while retaining full catalytic activity without FBP as the FBP-activated WT (Allen & Holbrook, 2000). In the present study, we showed that the single mutation Gln189Leu can keep the tetrameric structure without FBP, however, without improving substrate affinity (Supplementary video V3 & Table 2). This finding indicates that leucine-based tetramerization is insufficient to fully restore affinity toward pyruvate without FBP. FBP is essential for triggering conformational changes that propagate to the catalytic site, which, in turn, enhances the enzyme's affinity for pyruvate. One possible explanation is that hydrophobic interactions introduced by leucine on the *β*H from the *P*-axis-related subunits are responsible for tetrameric maintenance but fail to trigger the propagation of internal structural changes. The mutations Arg104Cys, located on the *α*D/E helix, and Asn293Ser, positioned at the N-terminal of *α*H in the triple mutant, most likely contribute to an FBP-like conformational change that governs the high affinity for both the substrate and the cofactor.

3.3 | A single mutation located in the interface increases substrate inhibition

Inhibition of LDHs by pyruvate occurs through the formation of a dead-end ternary complex involving LDH, NAD^+, and pyruvate (Burgner & Ray, 1978; Wilton, 1979). This non-productive complex forms when a holoenzyme with a non-protonated active-site histidine binds an enol form of pyruvate. A covalent bond is then formed between the nicotinamide ring of NAD^+ and the pyruvate moiety, preventing the release of NAD^+ from the enzyme (Gutfreund et al., 1968). Substrate inhibition of LDHs is intriguing from both scientific and biotechnological perspectives, as it offers potential insights into enzyme regulation and opportunities for industrial applications.

Substrate inhibition can be measured only in the presence of FBP because it enhances the affinity for pyruvate (Table 2). Thus, successful attempts to reduce inhibition were by impairing the affinity of NADH and pyruvate (Binay & Karagüler, 2007; Eszes et al., 1996; Hewitt et al., 1997; Hewitt et al., 1999). For example, a non-intuitive, single amino acid replacement, Ser163Leu, significantly reduced substrate inhibition (Hewitt et al., 1999). This mutation decreases the affinity of pyruvate toward LDH:NAD^+ complex, even though Ser163 interacts with the cofactor (Eszes et al., 1996). The role of Ser163 appears to orient the nicotinamide group of the cofactor thus further affecting the pyruvate binding (Eszes et al., 1996).

Here, we demonstrate that substrate inhibition can be enhanced by the Gln189Leu substitution located at the *P*-axis interface, which is 23 Å away from the ligand binding sites. The increased inhibition observed in the Gln189Leu mutant cannot be explained solely by higher substrate affinity. Kinetic analysis shows that while both the WT and mutant enzymes exhibit similar substrate affinity (K_m values 0.5 mM and 0.8 mM, respectively) in the presence of FBP, the Gln189Leu mutant shows a 10-fold lower K_i value, with minimal effect on the catalytic rate. While the precise mechanism of substrate (pyruvate) inhibition is the focus of a separate study, our results suggest that leucine at position 189 may contribute to further stabilization of the unproductive LDH-NAD^+-pyruvate complex, induced by FBP.

3.4 | Thermodynamics of cofactors binding

The binding of NADH to GsLDH was previously measured using an indirect method based on fluorescence spectroscopy, resulting in similar dissociation constant (K_d) values of 1.5–2 μM, both in the presence and absence of FBP (Clarke, Atkinson, et al., 1985). In this study, we determined the K_d of NADH using ITC, obtaining a value of 1.2 μM in the presence of FBP. However, in the absence of FBP, the enthalpy change was too low to be detected by ITC.

These results suggest that in the presence of FBP, the enthalpic contribution is significantly higher, consistent with the fact that FBP enhances hydrogen-bond formations. These interactions stabilize and orient the nicotinamide-ribose moiety in a productive conformation, facilitating high-affinity binding of pyruvate (Koide et al., 1992).

Fluorescence measurements indicate that NADH binds to the dimeric form (without FBP) of the protein with similar affinity ($K_d \sim 1.5$ μM), which contradicts the ITC results (Clarke, Atkinson, et al., 1985). This suggests that in the absence of FBP, the interaction is primarily entropically driven rather than enthalpically. Upon FBP binding, the conformation of NADH from the syn- (where the nicotinamide and adenine rings are on the same side of the ribose-phosphate backbone) shifts to the anti-conformation (where the two rings are on opposite sides of the backbone), minimizing steric hindrance between the bulky rings and promoting a more favorable binding interaction (Taguchi, 2017).

4 | CONCLUSIONS

Our study demonstrates that GsLDH oligomerization alone is insufficient for allosteric responsiveness; instead, specific interactions and conformational changes induced by the allosteric activator FBP are essential. Using experimental and computational approaches, we show that FBP is crucial for cofactor binding, optimizing the pyruvate site, and enhancing substrate affinity. FBP stabilizes key residues and affects three critical regions on the *P*-axis interface: (1) Asn170, which orients toward Ile255 across the dimer interface; (2) Lys60 and His250 at structural junctions; and (3) a hydrophobic loop (Ala190-Val194) that shifts the conformation without FBP. These features adopt distinct, stable conformations only in the presence of FBP. The Gln189Leu mutant retains a tetrameric form but lacks allosteric behavior, with FBP enhancing substrate inhibition. ITC analysis confirms that NADH binding ($K_d = 1.2$ μM) is FBP-dependent and enthalpically driven, suggesting that FBP facilitates a stabilizing hydrogen-bond network.

These insights expand our understanding of allosteric regulation and hold significant biotechnological relevance. GsLDH is widely used in high-temperature bioprocesses and diagnostics; understanding its allosteric control provides a foundation for rational engineering. Targeting specific residues involved in FBP-mediated activation offers opportunities to modulate enzyme responsiveness for improved yield, process control, and robustness. Moreover, our combined computational–experimental strategy presents a scalable approach for designing custom-regulated biocatalysts in other industrial enzymes.

5 | MATERIALS AND METHODS

5.1 | Cloning, expression, site directed mutagenesis, and purification of LDH proteins

The *Geobacillus stearothermophilus ldh* gene (accession number M19396, UniProt P00344) cloned into the pET28a vector (Novagen) was synthetically ordered from Twist Bioscience. The gene was amplified by PCR using primers (Table 4) designed for in-frame cloning into the T7 polymerase expression vector pET9d (pET9d-GsLDH). The primers included six histidine codons to produce N-terminal His-tagged protein products. The triple mutant Arg104Cys/Gln189Leu/Asn293Ser and single Gln189Leu mutant were constructed by the overlap extension PCR method (Hussain & Chong, 2016) using pET9d-GsLDH as a template and primers shown in Table 4. The mutated genes were sequenced to confirm that only the desired mutations were inserted.

For overexpression, the plasmid pET9d-GsLDH was transformed into *E. coli* BL21(DE3) (Novagen) and grown overnight (500 mL medium in a well-shaken 2 L baffled flasks at 37°C) in terrific broth medium containing kanamycin (25 μg/mL). Following overnight growth (typical final turbidity of OD_{600} 12) the cells were harvested, resuspended in 45 mL of buffer (20 mM Tris–HCl pH 7.5, 500 mM NaCl, 2.5% glycerol, 0.5 mM $CaCl_2$, and 20 mM imidazole), disrupted by two passages through an EmulsiFlex-C3 homogenizer (Avestin, Inc., Ottawa, Canada), and centrifuged (16,000 g for 20 min) to obtain a soluble extract. The soluble sample was incubated at 50°C for 15 min and centrifuged (16,000 g for 20 min). The clear supernatant after centrifugation was then uploaded on Histrap column (GE Health Care) using AKTA Prime Plus FPLC System. The GsLDH proteins were eluted by the buffer (20 mM Tris–HCl pH 7.5, 500 mM NaCl, 2.5% glycerol, 0.5 mM $CaCl_2$, and 500 mM imidazole) and appeared as a distinct protein peak, which was then collected and dialyzed over-night against 4 L of 20 mM Tris–HCl pH 7.5, 500 mM NaCl, 2.5% glycerol and 0.5 mM $CaCl_2$.

5.2 | Kinetic studies

GsLDH activity was measured by monitoring the decrease in absorbance at 340 nm, corresponding to NADH consumption. The reaction mixture consisted of 20 mM Bis-Tris HCl buffer (pH 6.5), 10 nM purified enzyme, 1 mM NADH, and 5 mM FBP. The reaction was initiated by adding pyruvate at concentrations ranging from 0.075 to 40 mM. Kinetic parameters were determined by nonlinear regression analysis using OriginPro 2024. In the presence of FBP, the WT, single mutant Gln189Leu, and triple mutant Arg104Cys/Gln189Leu/Asn293Ser exhibited substrate inhibition with increasing pyruvate concentrations. The Michaelis–Menten equation with substrate inhibition $V = V_{max}\ S/[K_m + S\ (1 + S/K_i)]$ was used to calculate the maximum velocity (V_{max}), the Michaelis constant of pyruvate (K_m) and the substrate inhibition constant (K_i).

In the absence of FBP, the dependence of initial reaction velocities of WT and single mutant Gln189Leu

TABLE 4 Oligonucleotides used in this study.

Primer name	Sequence (5′–3′)
*Nco*I_Fwr[a]	CAGAATCCATGGCACATCACCATCACCATCATAAGAATAACG
*Bam*HI_Rev[a]	CTAAGCTGGATCCTTAGCGGGTGAATGCCCGT
Arg104Cys_Fwr[b]	TTGATAAGAATATAGCGATCTTTtgcAGCATTGTGGAATC
Arg104Cys_Rev[b]	CATAACAGATTCCACAATGCTgcaAAAGATCGCTATATT
Gln189Leu_Fwr[b]	CCGAGTTGCCTGTGTGGTCCctgGCGTACATAGGAGTT
Gln189Leu_Rev[b]	ATTGGCATAACTCCTATGTACGCcagGGACCACACAGGC
Asn293Ser_Fwr[b]	GAAGTTATTGAGATCGAGCTGagcGACGATGAG
Asn293Ser_Rev[b]	GTTCTTCTCATCGTCgctCAGCTCGATCTCAA

[a]Restriction sequences *Nco*I and *Bam*HI are underlined.
[b]The codons of target corresponding mutations were marked in lowercase.

on pyruvate concentrations exhibited a sigmoidal curve. Therefore, the Hill equation $V = V_{max}\ S^n/(K_{0.5}{}^n + S^n)$ was used instead, where $K_{0.5}$ is the half-saturation constant, and n is the Hill coefficient. For the triple mutant Arg104Cys/Gln189Leu/Asn293Ser, since a sigmoidal curve was not obtained, a standard Michaelis–Menten equation $V = V_{max}\ S/(K_m + S)$ was applied.

5.3 | Size exclusion chromatography

To determine the oligomeric state, GsLDH variants were separated by a size exclusion column using an ÄKTA-Avant system (GE healthcare) equipped with a Superdex 200 Increase 10/300 GL column of 24 mL total volume. Protein samples (4 μM, 0.1 mL) were applied onto the column and eluted at room temperature with a solution consisting of 50 mM Tris–HCl buffer pH 7.5, 500 mM NaCl and 0.5 mM $CaCl_2$, at a flow rate of 0.5 mL/min. Molecular weights were determined from regression analysis of the log relative molecular weight (Mr) of protein standards as a function of K_{av}. K_{av}, the available partition coefficient, is defined as $(V_e - V_0)/(V_t - V_0)$, where V_e is the elution volume of the protein from the column, V_0 is the void number of the column, and V_t is the total column volume. The protein standards used were Thyroglobulin (Mr, 669,000), Ferritin (Mr, 440,000), Aldolase (Mr, 158,000), Conalbumin (Mr, 75,000) and Ovalbumin (Mr, 44,000) all from GH Healthcare.

5.4 | Microcalorimetry titration studies

Titration calorimetry measurements were performed with an ITC (MicroCal, iTC200). Protein solutions for ITC were dialyzed extensively overnight against a buffer containing 50 mM Tris–HCl (pH 7.5) and 100 mM NaCl. Ligand solutions of NAD^+ and NADH were prepared by dilution with the protein dialysis buffer. Protein samples were prepared with FBP and pyruvate and incubated overnight. Aliquots (1.5 μL) of the ligand solution at 10 times the molar concentration of the binding site were added to the reaction cell containing 25 μM protein solution by the controlled action of a rotating stirrer-syringe. The heat of dilution was determined to be negligible in separate titrations of the ligand into the buffer solution.

Calorimetric data analysis was carried out with the ORIGIN 7.0 software (MicroCal) and presented by thermograms and binding isotherms. Binding parameters, including the number of binding sites (N), the binding constant (K_B, [M^{-1}]), and the binding enthalpy (ΔH_B, [kcal/mol]) of bound ligand, were determined by fitting the experimental binding isotherms. The binding constant K_B was extracted by the slope of the isotherm at the equivalence point and the dissociation constant K_d is the reciprocal of the K_B.

5.5 | Statistical analysis

All experiments including kinetic studies, size exclusion chromatography and ITC were performed in three repetitions, and the results are presented as the form of mean ± standard deviation. Statistical analysis was performed using the OriginPro (Version 2025. OriginLab Corporation, Northampton, MA, USA) with ANOVA programme, followed by Tukey's Honestly Significant Difference test for multiple comparisons. A significance level of p-value <0.05 was applied to determine statistically meaningful variations.

5.6 | Structure preparation for MD simulations

The coordinates of substrate pyruvate were prepared by modifying oxamic acid (OXM) from PDB 1LDN using the software VMD, while the coordinates of the allosteric activator FBP and apo structure of GsLDH tetramer were directly extracted from PDB 1LDN. All ligands were visualized by ChimeraX to ensure that they were

properly located at the correct position within the LDH tetramer. The protein structure complex was uploaded to the APBS web server to estimate residue protonation states (pKa) at pH 7. The resulting output was visualized in VMD and further processed to adjust the protonation status of residues such as histidine within the tetramer.

5.7 | MD simulations

MD simulations were performed by the program Amber20. Two constructs of GsLDH: allosteric activator FBP bound and unbound protein were prepared for MD simulation. The GsLDH tetramer was described by amber ff14SB protein force field. The ligands' GAFF (the General Amber Force Field) atom types and parameters were determined and prepared by the antechamber tool and LEaP program from AmberTools23, respectively. The protein complexes were dissolved in TIP3P water (Jorgensen et al., 1983), while sodium ions were added to maintain the electroneutrality of the system.

After parameterization, a four-cycle energy minimization was performed for each protein complex. In the first cycles (1500 steps), all the protein atoms were fixed by a harmonic potential with a force constant of 50 kcal·(mol Å^2)$^{-1}$, allowing the ligands and water molecules to move. In the second cycle (2500 steps), the restraints were applied to only the protein backbone while the side chain of the residues were able to relax. In the third cycle (1500 steps), the force constant was reduced from 50 to 20 kcal·(mol Å^2)$^{-1}$ while in the fourth cycle (15,000 steps) the entire system was allowed to minimize without any restraints.

The minimized system first underwent heating from 0 to 310 K in the NVT ensemble (constant volume) for 50 ps and then equilibrated in NPT conditions (constant pressure) for 50 ps. Finally, MD simulation production was carried on at a constant temperature (310 K) using a Langevin thermostat with a collision frequency of 1 ps^{-1} and at a constant pressure (1 atm) using a Berendsen thermostat with isotropic position scaling. The period of each MD simulation was 500 ns, and the coordinates information was sampled every 1000 steps to the output file (NTPR) and trajectory file (NTWX), which contain 250,000 frames. The SHAKE algorithm was set to constrain the bonds involving hydrogen. The Particle Mesh Ewald method (Darden et al., 1993) was used to determine long-range electrostatic interactions, while non-bonded interactions were truncated at 10.0 Å. Each complex was simulated in three independent replicates, and all simulations were conducted with AMBER20 on GPU using the pmemd. CUDA engine (Götz et al., 2012; Salomon-Ferrer et al., 2013).

5.8 | Data analysis

The output trajectory files were processed by cpptraj program in amber20 to calculate the distance between residues, hydrogen bonds and atomic positional fluctuations. The distance between two histidine residues on FBP-binding stie was calculated based on the histidine side chain's heavy atoms (without hydrogen). A hydrogen bond was defined if the donor–acceptor distances were within 3.0 Å and the donor–hydrogen acceptor angles cutoff was 135° by default. The atomic positional fluctuations (also referred to as RMSF) calculation was performed after fitting to the first structure. The enthalpy of binding and per residue decomposition of enthalpy were calculated using the mmpbsa.py script from the AmberTools package, utilizing 10,000 frames extracted from the MD trajectory. Analysis of rotamers was conducted using the MDavocado tool (Gomaz et al., 2024), which identifies residues exhibiting distinct behaviors in MD simulations. The focus of the analysis is on the overall distribution of main-chain and side-chain torsion angles throughout the trajectory, visualized through Ramachandran plots (φ–ψ diagrams) and Janin plots ($\chi1$–$\chi2$ diagrams). The dihedral angles (φ, ψ, $\chi1$, $\chi2$) of the identified residues were presented as the average of the respective angle throughout the whole simulation. The videos showing dimerization process and tetramer maintenance of GsLDH were made from the MD simulation trajectory files by Chimera1.17.3.

AUTHOR CONTRIBUTIONS

Hanfeng Cai: Investigation; writing – original draft; methodology; formal analysis; data curation; validation. **Smadar Shulami:** Investigation; formal analysis; methodology; writing – original draft. **Zoran Štefanić:** Writing – review and editing; software; investigation; methodology. **Tomica Hrenar:** Investigation; writing – review and editing; software; methodology. **Aleksandra Maršavelski:** Writing – original draft; investigation; methodology; formal analysis; supervision; funding acquisition; resources. **Ayelet Fishman:** Conceptualization; funding acquisition; writing – review and editing; supervision; validation; project administration.

ACKNOWLEDGMENTS

This work was supported by the ISF grant 1372/24 and COST Action CA21162. H.C. acknowledges the Short-Term Scientific Missions (STSM) grant from COST Action CA21162. Computational experiments were performed using resources from the Computational Center of the Department of Chemistry, University of Zagreb and the SUPEK supercomputer at the University Computing Centre (SRCE). A.M. acknowledges the Development Research Support (NextGenerationEU) for the project Enzyme Engineering for sustainable recycling of bioplastics (NPOO.C3.2.R2-I1.06.0041). T. H.

acknowledges the support of project CluK co-financed by the Croatian Government and the European Union through the European Regional Development Fund–Competitiveness and Cohesion Operational Programme (Grant KK.01.1.1.02.0016). Z. Š. acknowledges grant IP-2019-04-6764, funded by the Croatian Science Foundation.

DATA AVAILABILITY STATEMENT

The data that support the findings of this study are available from the corresponding author upon reasonable request.

ORCID

Zoran Štefanić https://orcid.org/0000-0002-3486-4291
Ayelet Fishman https://orcid.org/0000-0002-1644-9377

REFERENCES

Allen SJ, Holbrook JJ. Production of an activated form of *Bacillus stearothermophilus* L-2-hydroxyacid dehydrogenase by directed evolution. Protein Eng Des Sel. 2000;13(1):5–7.

Arai K, Ichikawa J, Nonaka S, Miyanaga A, Uchikoba H, Fushinobu S, et al. A molecular design that stabilizes active state in bacterial allosteric l-lactate dehydrogenases. J Biochem. 2011;150(5):579–91.

Arai K, Ishimitsu T, Fushinobu S, Uchikoba H, Matsuzawa H, Taguchi H. Active and inactive state structures of unliganded *Lactobacillus casei* allosteric L-lactate dehydrogenase. Proteins. 2010;78(3):681–94.

Aslan AS, Birmingham WR, Karagüler NG, Turner NJ, Binay B. Semi-rational design of *Geobacillus stearothermophilus* L-lactate dehydrogenase to access various chiral α-hydroxy acids. Appl Biochem Biotechnol. 2016;179(3):474–84.

Astore MA, Pradhan AS, Thiede EH, Hanson SM. Protein dynamics underlying allosteric regulation. Curr Opin Struct Biol. 2024;84:102768.

Bertrand Q, Coquille S, Iorio A, Sterpone F, Madern D. Biochemical, structural and dynamical characterizations of the lactate dehydrogenase from *Selenomonas ruminantium* provide information about an intermediate evolutionary step prior to complete allosteric regulation acquisition in the super family of lactate and malate dehydrogenases. J Struct Biol. 2023;215(4):108039.

Binay B, Karagüler NG. Attempting to remove the substrate inhibition of L-lactate dehydrogenase from *Bacillus stearothermophilus* by site-directed mutagenesis. Appl Biochem Biotechnol. 2007;141(2):265–72.

Binay B, Sessions RB, Karagüler NG. A double mutant of highly purified *Geobacillus stearothermophilus* lactate dehydrogenase recognises l-mandelic acid as a substrate. Enzyme Microb Technol. 2013;52(6–7):393–9.

Binay B, Shoemark DK, Sessions RB, Clarke AR, Karaguler NG. Increasing the substrate specificity of *Bacillus stearothermophillus* lactate dehydrogenase by DNA shuffling. Biochem Eng J. 2009;48(1):118–23.

Brunori M, Miele AE. Modulation of allosteric control and evolution of hemoglobin. Biomolecules. 2023;13(3):572.

Burgner JW, Ray WJ. Mechanistic study of the addition of pyruvate to NAD^+ catalyzed by lactate dehydrogenase. Biochemistry. 1978;17(9):1654–61.

Cameron AD, Roper DI, Moreton KM, Muirhead H, Holbrook JJ, Wigley DB. Allosteric activation in *Bacillus stearothermophilus* lactate dehydrogenase investigated by an x-ray crystallographic analysis of a mutant designed to prevent tetramerization of the enzyme. J Mol Biol. 1994;238(4):615–25.

Chen J, Thirumalai D. Interface residues that drive allosteric transitions also control the assembly of L-lactate dehydrogenase. J Phys Chem B. 2018;122(49):11195–205.

Clarke AR, Atkinson T, Campbell JW, Holbrook JJ. The assembly mechanism of the lactate dehydrogenase tetramer from *Bacillus stearothermophilus*; the equilibrium relationships between quaternary structure and the binding of fructose 1,6-biphosphate, NADH and oxamate. Biochim Biophys Acta (BBA)—Protein Struct Mol Enzymol. 1985;829(3):387–96.

Clarke AR, Waldman ADB, Munro I, Holbrook JJ. Changes in the state of subunit association of lactate dehydrogenase from *Bacillus stearothermophilus*. Biochim Biophys Acta (BBA)—Protein Struct Mol Enzymol. 1985;828(3):375–9.

Clarke AR, Wigley DB, Barstow DA, Chia WN, Atkinson T, Holbrook JJ. A single amino acid substitution deregulates a bacterial lactate dehydrogenase and stabilizes its tetrameric structure. Biochim Biophys Acta (BBA)—Protein Struct Mol Enzymol. 1987;913(1):72–80.

Coquille S, Pereira CS, Roche J, Santoni G, Engilberge S, Brochier-Armanet C, et al. Allostery and evolution: a molecular journey through the structural and dynamical landscape of an enzyme super family. Mol Biol Evol. 2025;42(1):msae265.

Darden T, York D, Pedersen L. Particle mesh Ewald: an N·log (N) method for Ewald sums in large systems. J Chem Phys. 1993;98(12):10089–92.

Eszes CM, Sessions RB, Clarke AR, Moreton KM, Holbrook JJ. Removal of substrate inhibition in a lactate dehydrogenase from human muscle by a single residue change. FEBS Lett. 1996;399(3):193–7.

Frieden C. Treatment of enzyme kinetic data. J Biol Chem. 1967;242(18):4045–52.

Gomaz B, Pandini A, Maršavelski A, Štefanić Z. MDavocado: analysis and visualization of protein motion by time-dependent angular diagrams. J Chem Inf Model. 2024;64(15):5742–8.

Götz AW, Williamson MJ, Xu D, Poole D, Le Grand S, Walker RC. Routine microsecond molecular dynamics simulations with AMBER on GPUs. 1. Generalized born. J Chem Theory Comput. 2012;8(5):1542–55.

Gutfreund H, Cantwell R, McMurray CH, Criddle RS, Hathaway G. The kinetics of the reversible inhibition of heart lactate dehydrogenase through the formation of the enzyme–oxidized nicotinamide–adenine dinucleotide–pyruvate compound. Biochem J. 1968;106(3):683–7.

Hewitt CO, Eszes CM, Sessions RB, Moreton KM, Dafforn TR, Takei J, et al. A general method for relieving substrate inhibition in lactate dehydrogenases. Protein Eng, Des Sel. 1999;12(6):491–6.

Hewitt CO, Sessions RB, Dafforn TR, Holbrook JJ. Protein engineering tests of a homology model of plasmodium falciparum lactate dehydrogenase. Protein Eng Des Sel. 1997;10(1):39–44.

Hussain H, Chong NFM. Combined overlap extension PCR method for improved site directed mutagenesis. Biomed Res Int. 2016;2016(1):8041532.

Jorgensen WL, Chandrasekhar J, Madura JD, Impey RW, Klein ML. Comparison of simple potential functions for simulating liquid water. J Chem Phys. 1983;79(2):926–35.

Koide S, Yokoyama S, Matsuzawa H, Miyazawa T, Ohta T. Conformational equilibrium of an enzyme catalytic site in the allosteric transition. Biochemistry. 1992;31(23):5362–8.

Kotik M, Zuber H. Evidence for temperature-dependent conformational changes in the L-lactate dehydrogenase from Bacillus stearothermophilus. Biochemistry. 1992;31(34):7787–95.

Lazim R, Suh D, Lee JW, Vu TNL, Yoon S, Choi S. Structural characterization of receptor–receptor interactions in the allosteric modulation of G protein-coupled receptor (GPCR) dimers. Int J Mol Sci. 2021;22(6):3241.

Martinez-Vaz BM, Howard AL, Jamburuthugoda VK, Callahan KP. Insights into the regulation of malate dehydrogenase: inhibitors, activators, and allosteric modulation by small molecules. Essays Biochem. 2024;68(2):173–81.

McCullagh M, Zeczycki TN, Kariyawasam CS, Durie CL, Halkidis K, Fitzkee NC, et al. What is allosteric regulation? Exploring the exceptions that prove the rule! J Biol Chem. 2024;300(3): 105672.

Monod J, Wyman J, Changeux JP. On the nature of allosteric transitions: a plausible model. J Mol Biol. 1965;12(1):88–118.

Nichol LW, Frieden C. Protein–protein interactions. New York: Wiley; 1981.

Nichol LW, Jackson WJH, Winzor DJ. A theoretical study of the binding of small molecules to a polymerizing protein system. A model for allosteric effects*. Biochemistry. 1967;6(8):2449–56.

Nie B, Lodewyks K, Deng H, Desamero RZB, Callender R. Active-loop dynamics within the michaelis complex of lactate dehydrogenase from *Bacillus stearothermophilus*. Biochemistry. 2016; 55(27):3803–14.

Pasti AP, Rossi V, Di Stefano G, Brigotti M, Hochkoeppler A. Human lactate dehydrogenase a undergoes allosteric transitions under pH conditions inducing the dissociation of the tetrameric enzyme. Biosci Rep. 2022;42(1):BSR20212654.

Rennie ML, Chaugule VK, Walden H. Modes of allosteric regulation of the ubiquitination machinery. Curr Opin Struct Biol. 2020;62:189–96.

Robin AY, Brochier-Armanet C, Bertrand Q, Barette C, Girard E, Madern D. Deciphering evolutionary trajectories of lactate dehydrogenases provides new insights into allostery. Mol Biol Evol. 2023;40(10):msad223.

Salomon-Ferrer R, Götz AW, Poole D, Le Grand S, Walker RC. Routine microsecond molecular dynamics simulations with AMBER on GPUs. 2. Explicit solvent particle mesh Ewald. J Chem Theory Comput. 2013;9(9):3878–88.

Taguchi H. The simple and unique allosteric machinery of *Thermus caldophilus* lactate dehydrogenase. In: Atassi MZ, editor. Protein Reviews. Volume 17. Singapore: Springer; 2017. p. 117–45.

Thirumalai D, Hyeon C, Zhuravlev PI, Lorimer GH. Symmetry, rigidity, and allosteric signaling: from monomeric proteins to molecular machines. Chem Rev. 2019;119(12):6788–821.

Uchikoba H, Fushinobu S, Wakagi T, Konno M, Taguchi H, Matsuzawa H. Crystal structure of non-allosteric L-lactate dehydrogenase from *lactobacillus pentosus* at 2.3 Å resolution: specific interactions at subunit interfaces. Proteins. 2002;46(2): 206–14.

Wilton DC. The mechanism of adduct formation between NAD^+ and pyruvate bound to pig heart lactate dehydrogenase. Biochem J. 1979;177(3):951–7.

Wu N, Barahona M, Yaliraki SN. Allosteric communication and signal transduction in proteins. Curr Opin Struct Biol. 2024;84:102737.

SUPPORTING INFORMATION

Additional supporting information can be found online in the Supporting Information section at the end of this article.

How to cite this article: Cai H, Shulami S, Štefanić Z, Hrenar T, Maršavelski A, Fishman A. Allosteric regulation of L-lactate dehydrogenase: Beyond effector-mediated tetramerization. Protein Science. 2025;34(7):e70206. https://doi.org/10.1002/pro.70206